Manipulation of optical response in transition metal dichalcogenides by magnetic proximity effects and strain

Yueyue Wang, Zhihui Chen, Xinyu Cheng, Xiaolin Su, Peng Liu, Fanhao Jia, Ruixue Li, Yuan Li,* and Gaofeng Xu†
Department of Physics, Hangzhou Dianzi University, Hangzhou, Zhejiang 310018, China

(Received 20 January 2024; revised 1 May 2024; accepted 2 July 2024; published 15 July 2024)

Efficient manipulation of the optical response of two-dimensional (2D) semiconductors, dominated by excitons due to strong electron-hole Coulomb attraction, could give rise to both discoveries of emergent phenomena and implementation of optoelectronic devices. We propose a manipulation of the optical response of 2D semiconductors through combining magnetic proximity effects and strain, using a Janus type of monolayer (ML) transition-metal dichalcogenides (TMDs) for numerical illustration. Based on an effective Hamiltonian of a strained ML MoSSe on a magnetic substrate and a Bethe-Salpeter equation for an accurate description of excitons, we predict a mergence of A and B excitons at a critical strength of in-plane magnetic exchange field. Additionally, an enhanced tunability of the optical absorption spectra is demonstrated via the combination of magnetic exchange fields and strain. Our approach could be generally extended to other 2D semiconductors subject to magnetic proximity effects and strain.

DOI: 10.1103/PhysRevB.110.045425

I. INTRODUCTION

Since the discovery of graphene, atomically thin two-dimensional (2D) materials have evolved into a large family, exhibiting unique properties and offering intriguing opportunities for uncovering new physics alongside enormous potential applications [1–5]. Due to reduced dimensionality and weak dielectric screening, the optical response of 2D semiconductors is dominated by excitons, electron-hole pairs bound by Coulomb attraction [6]. Among various 2D semiconductors, monolayer (ML) transition-metal dichalcogenides (TMDs) MX_2 (M=Mo, W, X=S, Se, Te) have unique spin-valley coupling, direct band gaps, and strong light-matter coupling [7,8], rendering them well-suited platforms for both fundamental physics study and optoelectronic devices [9–15].

Efficient manipulation of optical response could enable both discoveries of emergent phenomena and implementation of optoelectronic devices for practical applications [16–19]. In particular, an effective combination of multiple approaches could offer unprecedented tunability. Proximity effects have been developed into a systematic approach of designing atomically thin materials with novel functionalities absent in pristine materials, since the atomic thickness lies well within the range of proximity effects [18,20]. In particular, magnetic proximity effects, whereby magnetization from a ferromagnetic penetrates its nonmagnetic material neighbor, have been exploited in the manipulation of spintronic, superconducting, valleytronic, excitonic, and topological phenomena in heterostructures [21–33].

Owing to substantial mechanical flexibility compared to bulk materials, strain serves as a powerful tool for tuning the electronic and optical properties of 2D materials [34]. For instance, a ML MoS_2 can stand strain above 10%, while most bulk semiconductors break at a much smaller strain below 1.5% [35]. Various techniques can be exploited to induce strain on ML materials, including bending, stretching, and elongation for homogeneous uniaxial strain [36–41], thermal expansion, and piezoelectric straining for biaxial strain [42–46].

We propose a joint manipulation of the optical response in ML TMDs, through varying magnetic exchange fields combined with strain. For numerical illustration, we examine a typical member of Janus TMDs, which are recently fabricated variation of TMDs of the form MXY with M=Mo, W and X, Y=S, Se, Te [47–49]. Due to the different chalcogen atoms above and below transition-metal atoms in Janus TMDs, the mirror-reflection symmetry is broken and the monolayers possess intrinsic out-of-plane dipole moments, unlike standard TMDs. Specifically, we consider a ML MoSSe on a magnetic and strain-tunable substrate, as shown in Figs. 1(a) and 1(b). The influence of exchange field (in-plane and out-of-plane) and strain to the band structure at the K valley is illustrated schematically in Fig. 1(c).

Following the introduction, in Sec. II we establish an effective model of the strained ML TMD on a magnetic substrate and set up a Bethe-Salpeter equation (BSE) to elucidate the electron-hole Coulomb interaction. In Sec. III, we demonstrate evolution of the absorption spectra under various magnetic exchange fields and strain. Conclusions are given in Sec. IV.

II. THEORETICAL FRAMEWORK

A strained ML TMD on a magnetic substrate can be described by the Hamiltonian $H_{\rm tot} = H_0 + H_{\rm ex} + H_{\rm R} + H_\epsilon$,

*Contact author: liyuan@hdu.edu.cn
†Contact author: xug@hdu.edu.cn

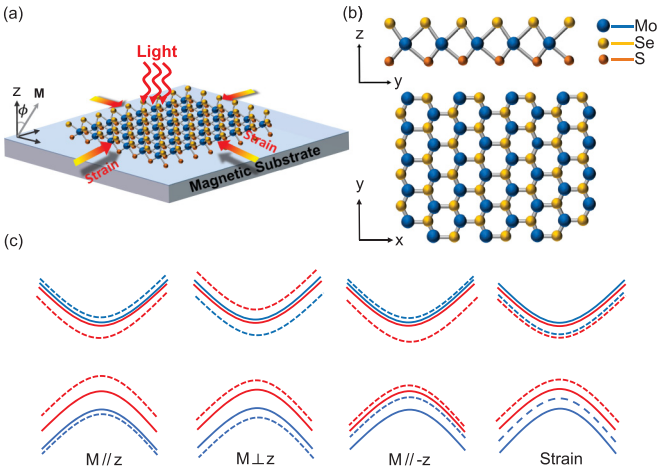

FIG. 1. (a) A strained ML TMD on a magnetic substrate. (b) Top and side views of ML MoSSe. (c) Influence of magnetic exchange fields along different directions and compressive strain to the single-particle band structure at the K valley. The band structure without exchange fields and strain is given in solid.

including a "bare" ML TMD term, a proximity-induced exchange term, Rashba spin-orbit coupling (SOC), and a strain term [50–55]. At the K/K' valleys, the Hamiltonian of a "bare" ML TMD is given by

$$H_0 = \hbar v_F(k_x\sigma_x\tau_z + k_y\sigma_y) + (E_g/2)\sigma_z + \tau_z s_z[\lambda_c(1+\sigma_z)/2 + \lambda_v(1-\sigma_z)/2], \quad (1)$$

where v_F is the Fermi velocity, E_g is the band gap without SOC, $\lambda_{c(v)}$ is the spin-splitting parameter of the conduction (valence) band CB (VB), and σ_i, τ_i, and s_i denote Pauli matrices for the orbital (CB or VB), valley, and spin degrees of freedom, respectively. For a magnetization of the substrate $\mathbf{M} = M\mathbf{n}$, the exchange term is

$$H_{\rm ex} = -\mathbf{n}\cdot\mathbf{s}[J_c(1+\sigma_z)/2 + J_v(1-\sigma_z)/2], \quad (2)$$

where $J_{c(v)}$ is the exchange splitting in the CB (VB). The Rashba SOC $H_{\rm R} = \lambda_R(s_y\sigma_x\tau_z - s_x\sigma_y)$ with λ_R the Rashba SOC parameter. Strain can be described by [54,55]

$$H_\epsilon = \delta_1(\epsilon_{xx}+\epsilon_{yy})\sigma_z + \delta_2[(\epsilon_{xx}-\epsilon_{yy})\sigma_x - 2\epsilon_{xy}\sigma_y], \quad (3)$$

where $\delta_{1,2}$ are spin-independent coefficients, and ϵ_{xx}, ϵ_{yy}, and ϵ_{xy} are parameters for x direction, y direction, and shear strain, respectively. In our model, electron-hole asymmetry and trigonal warping terms [55] are not included, which only have minor effects on the absorption spectra [56].

Based on the single-particle description, $H_{\rm tot}\eta^\tau_{n\boldsymbol{k}} = \epsilon^\tau_n(\boldsymbol{k})\eta^\tau_{n\boldsymbol{k}}$ with the energies ϵ^τ_n and the corresponding eigenstates $\eta^\tau_{n\boldsymbol{k}}$ in a valley τ, a generalized Bethe-Salpeter equation (BSE) can be developed to describe the many-body manifestation of the magnetic proximity effect [27,57,58]

$$\left[\Omega^\tau_S - \epsilon^\tau_c(\boldsymbol{k}) + \epsilon^\tau_v(\boldsymbol{k})\right]\mathcal{A}^{S\tau}_{vc\boldsymbol{k}} = \sum_{v'c'\boldsymbol{k}'} \mathcal{K}^\tau_{vc\boldsymbol{k},v'c'\boldsymbol{k}'}\mathcal{A}^{S\tau}_{v'c'\boldsymbol{k}'}, \quad (4)$$

where the band index $n = c(v)$ denotes one of the two CBs (VBs) in the given valley τ, Ω^τ_S is the energy of the exciton state $|\Psi^\tau_S\rangle = \sum_{vc\boldsymbol{k}}\mathcal{A}^{S\tau}_{vc\boldsymbol{k}}\hat{c}^\dagger_{\tau c\boldsymbol{k}}\hat{c}_{\tau v\boldsymbol{k}}|{\rm GS}\rangle$, and $\mathcal{A}^{S\tau}_{vc\boldsymbol{k}}$ is the coefficients. $\hat{c}^\dagger_{\tau c\boldsymbol{k}}$ ($\hat{c}_{\tau v\boldsymbol{k}}$) denotes the creation (annihilation) operator of an electron in a CB c (VB v) in the valley. $|{\rm GS}\rangle$ is the ground state with unoccupied CBs and fully occupied VBs. Note that we do not take into account intervalley scattering processes.

The interaction kernel contains direct and exchange terms, given by

$$\mathcal{K}^\tau_{vc\boldsymbol{k},v'c'\boldsymbol{k}'} = \mathcal{K}^{d,\tau}_{vc\boldsymbol{k},v'c'\boldsymbol{k}'} + \mathcal{K}^{{\rm x},\tau}_{vc\boldsymbol{k},v'c'\boldsymbol{k}'}, \quad (5)$$

$$\mathcal{K}^{d,\tau}_{vc\boldsymbol{k},v'c'\boldsymbol{k}'} = -\int d^2r d^2r' W(\boldsymbol{r}-\boldsymbol{r}')\left\{\left[\psi^\tau_{c\boldsymbol{k}}(\boldsymbol{r})\right]^\dagger\psi^\tau_{c'\boldsymbol{k}'}(\boldsymbol{r})\right\} \times\left\{\left[\psi^\tau_{v'\boldsymbol{k}'}(\boldsymbol{r}')\right]^\dagger\psi^\tau_{v\boldsymbol{k}}(\boldsymbol{r}')\right\}, \quad (6)$$

$$\mathcal{K}^{{\rm x},\tau}_{vc\boldsymbol{k},v'c'\boldsymbol{k}'} = \int d^2r d^2r' V(\boldsymbol{r}-\boldsymbol{r}')\left\{\left[\psi^\tau_{c\boldsymbol{k}}(\boldsymbol{r})\right]^\dagger\psi^\tau_{v\boldsymbol{k}}(\boldsymbol{r})\right\} \times\left\{\left[\psi^\tau_{v'\boldsymbol{k}'}(\boldsymbol{r}')\right]^\dagger\psi^\tau_{c'\boldsymbol{k}'}(\boldsymbol{r}')\right\}, \quad (7)$$

where $\psi^\tau_{c\boldsymbol{k}}(\boldsymbol{r})$ are the wave functions of the single-particle states with energies $\epsilon^\tau_n(\boldsymbol{k})$, $V(\boldsymbol{r})$ denotes the real-space Coulomb potential determined only by the dielectric environment, and $W(\mathbf{r})$ is the Coulomb potential including screening from free charge carriers. The single-particle states $\psi^\tau_{n\mathbf{k}}(\mathbf{r}) = \exp(i\mathbf{k}\cdot\mathbf{r})\eta^\tau_{n\mathbf{k}}/\sqrt{A}$, with A the unit area, are determined by $H_{\rm tot}\eta^\tau_{n\boldsymbol{k}} = \epsilon^\tau_n(\boldsymbol{k})\eta^\tau_{n\boldsymbol{k}}$. Insert $\psi^\tau_{n\boldsymbol{k}}(\mathbf{r})$ into Eqs. (6) and (7), and we get

$$\mathcal{K}^{d,\tau}_{vc\boldsymbol{k},v'c'\boldsymbol{k}'} = -\frac{W(\boldsymbol{k}-\boldsymbol{k}')f_{cc'}(\boldsymbol{k},\boldsymbol{k}')f_{v'v}(\boldsymbol{k}',\boldsymbol{k})}{A}, \quad (8)$$

$$\mathcal{K}^{X,\tau}_{vc\boldsymbol{k},v'c'\boldsymbol{k}'} = -\frac{V(\boldsymbol{k}-\boldsymbol{k}')f_{cv}(\mathbf{k},\mathbf{k})f_{v'c'}(\mathbf{k}',\mathbf{k}')}{A}, \quad (9)$$

where $f^\tau_{nn'}(\boldsymbol{k},\boldsymbol{k}') = [\eta^\tau_{n\boldsymbol{k}}]^\dagger\eta^\tau_{n'\boldsymbol{k}'}$ are form factors calculated from the single particle state. $W(\boldsymbol{k})$ and $V(\boldsymbol{k})$ are the Fourier transforms of $W(\boldsymbol{r})$ and $V(\boldsymbol{r})$. Due to the orthogonality of the eigenspinors $\eta^\tau_{n\boldsymbol{k}}$, $f^\tau_{cv}(\boldsymbol{k},\boldsymbol{k}) = 0$. Therefore, $\mathcal{K}^{X,\tau}_{vc\boldsymbol{k},v'c'\boldsymbol{k}'}$ vanishes. As a result, $\mathcal{K}^\tau_{vc\boldsymbol{k},v'c'\boldsymbol{k}'} = \mathcal{K}^{d,\tau}_{vc\boldsymbol{k},v'c'\boldsymbol{k}'}$ in our model.

The Coulomb potential $V(\boldsymbol{q})$ is determined by the dielectric environment and obtained by the Poisson equation. We consider a geometry where a ML TMD of thickness d and dielectric constant $\tilde{\varepsilon}$ is embedded in a top material (air) and a bottom material (magnetic substrate) with respective dielectric constants ε_t and ε_b. The Coulomb potential $V(\boldsymbol{q})$ between two electrons in the ML (xy plane) can be calculated as [59,60]

$$V(\boldsymbol{q}) = \frac{2\pi e^2}{q}\times\frac{(\tilde{\varepsilon}^2-\varepsilon_t\varepsilon_b) + (\tilde{\varepsilon}^2+\varepsilon_t\varepsilon_b)\cosh(qd) + \tilde{\varepsilon}(\varepsilon_t+\varepsilon_b)\sinh(qd)}{\tilde{\varepsilon}[(\tilde{\varepsilon}^2+\varepsilon_t\varepsilon_b)\sinh(qd) + \tilde{\varepsilon}(\varepsilon_t+\varepsilon_b)\cosh(qd)]}. \quad (10)$$

We consider the absorption in a semiconductor ground state, where the conduction bands are completely empty and all valence bands are occupied, then the two potentials coincide: $W(\boldsymbol{q}) = V(\boldsymbol{q})$.

TABLE I. Parameters used in numerical calculations.

Parameter	Value	Parameter	Value
E_g	2.01 eV	ϵ_t	1
v_F	5.43×10^5 m/s	ϵ_b	23.9
a_0	3.21 Å	$\tilde{\epsilon}$	8.67
λ_c	0.015 eV	J_c	0.1 eV
λ_v	−0.12 eV	J_v	0.085 eV
λ_R	0.05 eV	δ_1	−3.10 eV
d	3.25 Å	δ_2	2.29 eV

The optical response of the ML dominated by excitons can be described by the absorption

$$\alpha(\omega) = \frac{4e^2\pi^2}{c\omega}\frac{1}{A}\sum_{S\tau}\left|\sum_{vc\boldsymbol{k}}\mathcal{V}_{vc\boldsymbol{k}}\mathcal{A}^{S\tau}_{vc\boldsymbol{k}}\right|^2\delta\left(\hbar\omega-\Omega^{\tau}_{S}\right), \quad (11)$$

where ω is the frequency of light propagating in the negative **z** direction, and c is the speed of light. The velocity matrix elements are $\mathcal{V}^{\sigma^\pm}_{vc\boldsymbol{k}} = [\eta^{\tau}_{v\boldsymbol{k}}]^{\dagger}\hat{v}_{\pm}\eta^{\tau}_{c\boldsymbol{k}}$ for $\sigma^\pm$ circularly polarized light, with $\hat{v}_\pm = \frac{(\hat{v}_x \pm i\hat{v}_y)}{\sqrt{2}}$, and $\hat{v}_{x/y} = \frac{\partial H_{t\alpha}}{\partial(\hbar k_{x/y})}$. The δ function is implemented as a Lorentzian with broadening Γ.

III. RESULTS

We explore the optical response of a ML MoSSe on a magnetic substrate EuO under various exchange fields and strain. We employ reduced exchange couplings of $J_c = 100$ meV and $J_v = 85$ meV, guided by first-principles calculations demonstrating a giant proximity-induced exchange splitting [51]. The parameters used in our numerical calculations are summarized in Table I. Parameters related to the band structure can be obtained by fitting the band structure from first principles calculations [50–53,55].

In our model, the BSE [Eq. (4)] contains two conduction and two valence bands for a given valley τ. Intervalley coupling is neglected and excitons can be calculated for each valley separately. For numerical calculation of Eq. (4), we use a uniform $N \times N$ k grid with a spacing of $\Delta k = 2\pi/(Na_0)$ in each direction as well as an upper energy cutoff E_{cut}. To ensure convergence in our numerical calculations, we have used $N = 120$ and energy cutoff of 0.9 eV above the band gap; $E_{\text{cut}} = E_g/2 + 0.9$ eV. Convergence is confirmed, with $<1\%$ variation in the $1s$ binding energy from $N = 100$ to 120.

The direction and strength of the exchange field could be manipulated, for instance, by an external magnetic field, which proportionally tunes substrate magnetization and the associated proximity-induced exchange splitting [24]. It has also been reported to be controlled by an external electric field [61] or quantum confinement [62].

For convenience, we quantify the manipulation of the strength of the magnetic exchange field by assuming a fixed ratio between J_c and J_v as $J_c/J_v = 100/85$, introducing a parameter J such that $J_c = J$ and $J_v = 0.85J$. We show in Fig. 2 the absorption spectra of σ^+ circularly polarized light as J increases from 0 to 0.4 eV. Since absorption of σ^+ (σ^-) circularly polarized light occurs at the K (K') valley exclusively and an in-plane magnetic exchange field yields

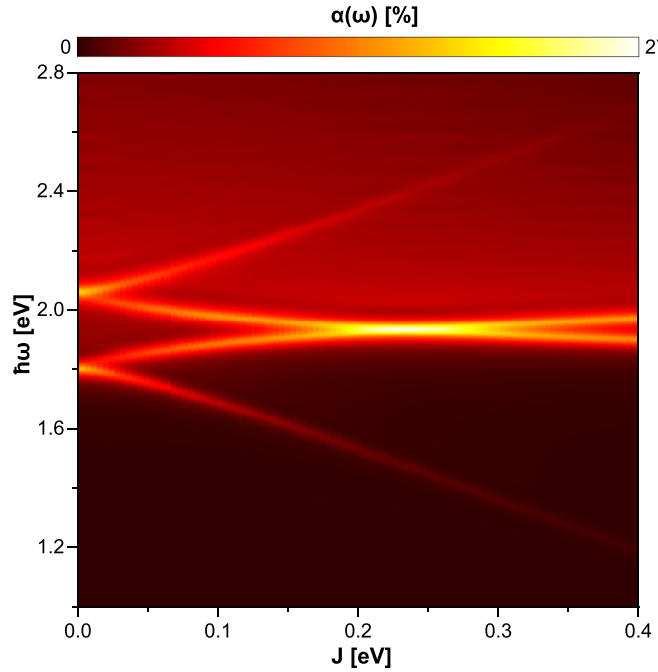

FIG. 2. Evolution of the σ^+ absorption spectra of a ML MoSSe as the strength of the in-plane magnetic exchange field increases. J_c and J_v are scaled with J as $J_c = J$, $J_v = 0.85J$.

symmetric $\sigma^\pm$ absorption spectra [6,27], we focus on the σ^+ absorption at the K valley.

Without the in-plane magnetic exchange field ($J = 0$), two bright excitons exist known as the A and B excitons, related to dipole-allowed transitions from the upper (A) and lower (B) valence bands. As the strength of the exchange field increases, each of the absorption peaks gradually split into two peaks, i.e., dark excitons below, and above A and B excitons turn into bright. As J increases, the A exciton blue shifts while the B exciton red shifts. In particular, the absorption peaks of the two excitons merges at $J \approx 0.25$ eV. As the exchange field increases further, the merged peak splits into two separate ones again, with growing energy splitting. Furthermore, while the lower dark exciton continuously red shifts, the upper dark exciton blue shifts, with their energy difference expanding with J. Consequently, the absorption spectra of a ML MoSSe can be manipulated substantially by the in-plane magnetic exchange field, tuning the energies and even the number of absorption peaks.

To understand such a phenomenon we examine the energy of excitons under an in-plane exchange field J, formally given by [27]

$$\hbar\omega^{\text{exc}}_{cv}(J) = \epsilon^{\tau}_{c}(J) - \epsilon^{\tau}_{v}(J) - E^{cv}_{b}(J), \quad (12)$$

where ϵ^{τ}_c and ϵ^{τ}_v are their respective single-particle band edges at valley τ, and E^{cv}_b is the binding energy of the $1s$ exciton mainly formed by CB c and VB v. The single-particle band edges can be calculated analytically without Rashba SOC ($\lambda_R = 0$) as

$$\epsilon^{\tau}_{c,\pm} = E_g/2 \pm \sqrt{J_c^2 + \lambda_c^2}, \quad (13)$$

$$\epsilon^{\tau}_{v,\pm} = -E_g/2 \pm \sqrt{J_v^2 + \lambda_v^2}, \quad (14)$$

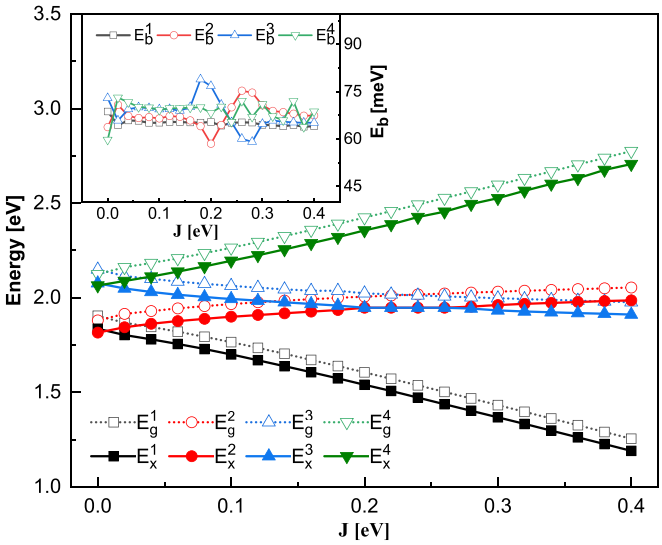

FIG. 3. Dependence of single-particle band gaps and excitonic absorption peak energies of ML MoSSe on the strength of magnetic exchange field. Inset: Corresponding exciton binding energies as functions of J.

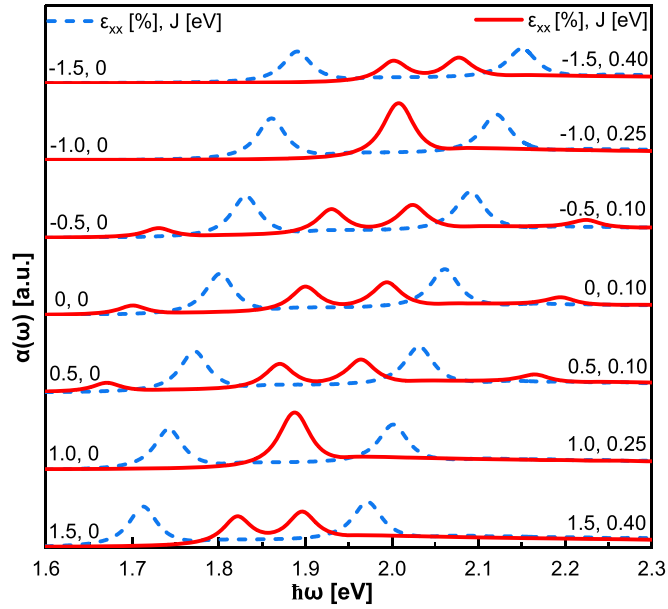

FIG. 4. Absorption spectra of ML MoSSe for a series of uniaxial strain and strengths of the in-plane exchange field. The dashed curves show the effects of strain without exchange fields ($J = 0$), while the solid curves show their joint effects.

for the band edges of two CBs and VBs, respectively. Therefore, the four sets of single-particle band gaps between different CBs and VBs are

$$E_g^N = E_g \pm \sqrt{J_c^2 + \lambda_c^2} \mp \sqrt{J_v^2 + \lambda_v^2}, \tag{15}$$

where $N = 1, 2, 3, 4$ labels gaps in an ascending order of energy in the absence of exchange field. In fact, the band edges are just slightly affected by a moderate Rashba SOC as we have numerically examined, therefore the analytical expressions are good approximations. Specifically, with the fixed scale between J_c and J_v, the gaps are $E_g^N = E_g \pm \sqrt{J^2 + \lambda_c^2} \mp \sqrt{0.85^2 J^2 + \lambda_v^2}$, which can be expanded with small J as $E_g^N \approx E_g \pm [\lambda_v + (0.85J)^2/2\lambda_v] \pm (\lambda_c + J^2/2\lambda_c)$, indicating clear trends with J. Since $|\lambda_v| \gg |\lambda_c|$ in ML TMDs, $J^2/2\lambda_c$ dominates the J dependence. Therefore we see that as J increases, E_g^2 (related to A excitons) increases while E_g^3 (related to B excitons) decreases. Consequently, the energy difference $\Delta E = E_g^2 - E_g^3$ decreases with J. In particular, ΔE vanishes at a specific strength of exchange field $J_0 = \sqrt{(\lambda_v^2 - \lambda_c^2)/(1 - 0.85^2)} \approx 0.23$ eV, and changes its sign with even larger J. In general, Eq. (15) implies that E_g^2 and E_g^3 become equal when the strengths of in-plane exchange field satisfy the relation $J_c^2 + \lambda_c^2 = J_v^2 + \lambda_v^2$. More specifically, we show J dependence of single-particle band gaps in Fig. 3 with numerical calculations including a finite Rashba SOC ($\lambda_R = 50$ meV). We indeed see a crossing of two gaps at around $J = 0.24$ eV, which is consistent with the analytical analysis. In addition, we show the J dependence of the exciton energies E_x^N (labeled in ascending order) in solid, which share similar trends as the gaps, as well as a crossing of the energies of the corresponding excitons near the same J values. Such a similarity between E_g^N and E_x^N is due to relatively stable exciton-binding energies against J, as shown in the inset of Fig. 3. Therefore, the manipulation of exciton energies by the in-plane exchange field, especially, the convergence and separation of A and B excitonic peaks, is due to effective tuning of the single-particle gaps by the strength of the exchange field.

Strain is ubiquitous in atomic heterostructures, which could have substantial effects on the properties of atomic monolayers. We further investigate the absorption spectra of ML MoSSe combining a series of uniaxial strain ε_{xx} from -1.5% to 1.5% ($\varepsilon_{yy} = 0$), and in-plane exchange fields with J from 0 to 0.40 eV, as shown in Fig. 4. We see that without the exchange field ($J = 0$), tensile strain leads to red shifts of the absorption peaks, while compressive strain leads to blue shifts, as expected. The three curves with $J = 0.10$ eV and $\varepsilon_{xx} = -0.5\%, 0, 0.5\%$, share similar features containing A and B peaks, as well as two weaker peaks brightened by the in-plane exchange field, with overall shifts of peak positions by strain. For $J = 0.25$ eV and $\varepsilon_{xx} = \pm 1.0\%$, A and B peaks merge into one, shifted more than 100 meV by strain. For even larger $J = 0.40$ eV, A and B peaks are recovered with smaller separation compared to cases with $J = 0.10$ eV, and the two peaks corresponding to formerly dark excitons become too weak to be visible. Besides, we have also examined cases with biaxial strain, which leads to similar but more significant effects than uniaxial strain. Therefore, a variety of absorption spectra with different energies, relative separations, and numbers of peaks can be achieved by a combination of strain and in-plane exchange fields.

Specifically, we show in Fig. 5 the dependence of the energies of A excitons on both uniaxial and biaxial strain for a series of in-plane exchange field $J/\text{eV} = 0, 0.1, 0.25, 0.4$. A exciton energies show roughly linear decrease with both uniaxial and biaxial strain and the redshift rates are close for different J. In particular, the redshift rate of biaxial strain is nearly twice that of uniaxial strain. For instance, the energy shift between $\varepsilon_{xx} = \pm 1.5\%$ is about 180 meV for uniaxial

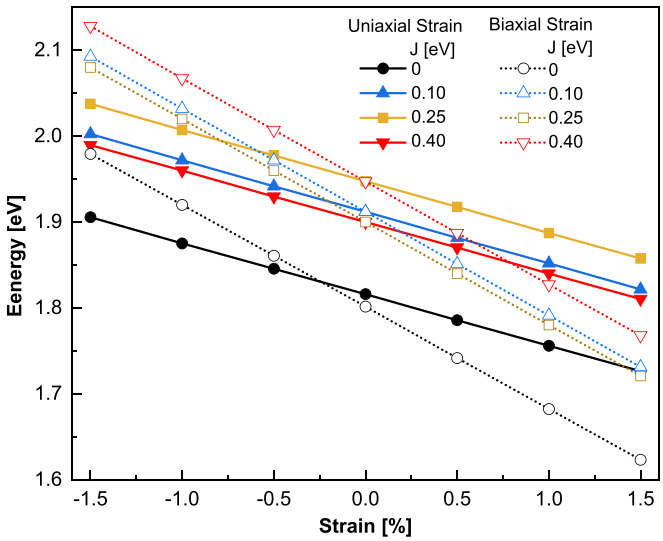

FIG. 5. The strain dependence of the energies of A excitons of ML MoSSe at the K valley under uniaxial (solid) and biaxial strain (dashed) for a series of in-plane exchange field $J/\text{eV} = 0, 0.1, 0.25, 0.4$.

strain, while that for biaxial strain ($\varepsilon_{xx} = \varepsilon_{yy} = \pm 1.5\%$) is about 360 meV. Unlike the linear dependence on strain, the dependence on J is nonmonotonic. The A exciton energies with $J = 0.25$ eV are greater than those with $J = 0.1$ and 0.40 eV under the same strain. Such a J dependence is also revealed in Fig. 2 for cases without strain. The A exciton energy can be tuned by the in-plane exchange field in a range of more than 200 meV, and the range can be 500 meV combined with strain.

In addition to in-plane exchange fields, we further investigate magnetic exchange fields along different directions. Figure 6 presents the band gaps, the energies of A excitons,

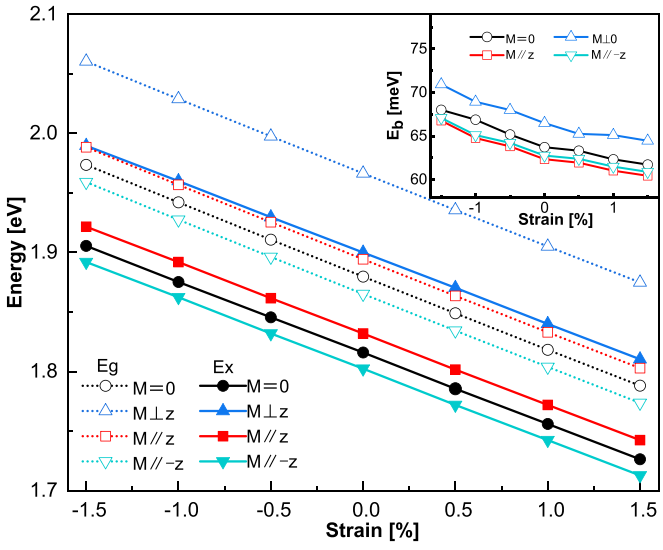

FIG. 6. The strain dependence of band gaps (dashed), the energies (solid) of the A excitons and binding energies (inset) at the K valley for cases without exchange field ($\mathbf{M} = 0$), with exchange field: strength $J = 0.1$ eV and substrate magnetization $\mathbf{M}$ along directions $\phi = 0, \pi/2, \pi$.

and corresponding exciton binding energies under uniaxial strain for cases without exchange field ($\mathbf{M} = 0$), and with exchange field ($J = 0.1$ eV) $\mathbf{M}$, along three representative directions $\mathbf{M}//\mathbf{z}$, $\mathbf{M} \perp \mathbf{z}$, and $\mathbf{M}//-\mathbf{z}$ ($\phi = 0, \pi/2, \pi$) [see Fig. 1(a)] at the K valley. Without exchange fields, the gaps and A exciton energies exhibit an approximately linear decrease with strain, consistent with theory and experiments [37,38]. Such a linear dependence remains unchanged under in-plane and out-of-plane exchange fields, with a similar redshift rate of about 60 meV per percent of uniaxial strain. Unlike in-plane exchange fields, out-of-plane exchange fields break valley degeneracy, with $\mathbf{M}$ along $\phi = 0$ ($\phi = \pi$) at the K' (K) valley equivalent to $\mathbf{M}$ along $\phi = \pi$ ($\phi = 0$) at the K (K') valley. Therefore, the strain dependence for $\mathbf{M}$ along $\phi = 0$ and $\phi = \pi$ at both valleys can be inferred. As shown in the inset, binding energies for all cases decline slightly with strain, which is related to a decrease of effective masses of the energy bands [46]. Consequently, the strain dependence of exciton energies is dominated by the band gaps, which scale with strain as $2\delta_1(\epsilon_{xx} + \epsilon_{yy})$ in the leading-order approximation, based on our analytical analysis of the gaps under out-of-plane exchange fields. Such a scaling relation is in alignment with numerical results of uniaxial strain ($\epsilon_{xx} \neq 0$ and $\epsilon_{yy} = 0$) in Fig. 6, as well as our additional calculation for biaxial strain ($\epsilon_{xx} = \epsilon_{yy}$), which exhibits qualitatively similar linear dependence but nearly doubled redshift rates. In the parameter regime considered here, the modifications of exciton binding energies by exchange fields and strain are relatively small. Therefore, the qualitative trends of the energies of excitonic absorption peaks could be implied from the dependence of single-particle gaps. The observed behavior of manipulation by exchange field and strain is not significantly affected by the Janus asymmetry. We have also numerically examined some other ML TMDs, such as MoS_2, which follow similar trends. However, Janus asymmetry leads to an intrinsic dipole moment in the out-of-plane direction, which allows further manipulation of its band gaps, Rashba SOC, and absorption spectra by external electric fields.

IV. CONCLUSIONS

To conclude, we have demonstrated the manipulation of optical response in ML TMDs through combinations of magnetic exchange fields and strain. Notably, we have predicted a mergence and separation of A and B excitonic peaks when the strength of the in-plane exchange field approaches and exceeds a critical value, which is understood via exchange-mediated modulation of relevant single-particle band gaps alongside relatively stable binding energies. Furthermore, enhanced tunability of ML TMD excitonic absorption is achievable by controlling the magnitude and orientation of magnetic exchange fields in conjunction with strain.

While a fixed J_c/J_v ratio was assumed for illustrative numerical calculations, the predicted phenomena persist for variable ratios. For ML Janus TMDs, which have nonzero out-of-plane dipole moments, the manipulation of optical response could be further combined with out-of-plane electric fields. Moreover, it is possible to extend our predictions beyond ML TMDs elucidated here to other 2D semiconductors. With advancing techniques in controlling magnetic exchange

fields and strain engineering, our prediction could be experimentally tested and exploited for a desired control of the optical response of 2D semiconductors.

ACKNOWLEDGMENT

This work has been supported by the National Natural Science Foundation of China (Grant No. 12104118).

[1] K. S. Novoselov, A. K. Geim, S. V. Morozov, D. Jiang, Y. Zhang, S. V. Dubonos, I. V. Grigorieva, and A. A. Firsov, Electric field effect in atomically thin carbon films, Science **306**, 666 (2004).

[2] A. K. Geim and I. V. Grigorieva, Van der Waals heterostructures, Nature (London) **499**, 419 (2013).

[3] X. Xu, W. Yao, D. Xiao, and T. F. Heinz, Spin and pseudospins in layered transition metal dichalcogenides, Nat. Phys. **10**, 343 (2014).

[4] B. W. H. Baugher, H. O. H. Churchill, Y. Yang, and P. Jarillo-Herrero, Optoelectronic devices based on electrically tunable p-n diodes in a monolayer dichalcogenide, Nat. Nanotechnol. **9**, 262 (2014).

[5] K. L. Seyler, P. Rivera, H. Yu, N. P. Wilson, E. L. Ray, D. G. Mandrus, J. Yan, W. Yao, and X. Xu, Signatures of moiré-trapped valley excitons in $MoSe_2/WSe_2$ heterobilayers, Nature (London) **567**, 66 (2019).

[6] G. Wang, A. Chernikov, M. M. Glazov, T. F. Heinz, X. Marie, T. Amand, and B. Urbaszek, *Colloquium:* Excitons in atomically thin transition metal dichalcogenides, Rev. Mod. Phys. **90**, 021001 (2018).

[7] K. F. Mak, C. Lee, J. Hone, J. Shan, and T. F. Heinz, Atomically thin MoS_2: A new direct-gap semiconductor, Phys. Rev. Lett. **105**, 136805 (2010).

[8] A. Splendiani, L. Sun, Y. Zhang, T. Li, J. Kim, C.-Y. Y. Chim, G. Galli, and F. Wang, Emerging photoluminescence in monolayer MoS_2, Nano Lett. **10**, 1271 (2010).

[9] J. Lee, S. Bearden, E. Wasner, and I. Žutić, Spin-lasers: From threshold reduction to large-signal analysis, Appl. Phys. Lett. **105**, 042411 (2014).

[10] S. Wu, S. Buckley, J. R. Schaibley, L. Feng, J. Yan, D. G. Mandrus, F. Hatami, W. Yao, J. Vučković, A. Majumdar, and X. Xu, Monolayer semiconductor nanocavity lasers with ultralow thresholds, Nature (London) **520**, 69 (2015).

[11] Y. Ye, Z. J. Wong, X. Lu, X. Ni, H. Zhu, X. Chen, Y. Wang, and X. Zhang, Monolayer excitonic laser, Nat. Photonics **9**, 733 (2015).

[12] Y. Li, J. Zhang, D. Huang, H. Sun, F. Fan, J. Feng, Z. Wang, and C. Z. Ning, Room-temperature continuous-wave lasing from monolayer molybdenum ditelluride integrated with a silicon nanobeam cavity, Nat. Nanotechnol. **12**, 987 (2017).

[13] M. Lindemann, G. Xu, T. Pusch, R. Michalzik, M. R. Hofmann, I. Žutić, and N. C. Gerhardt, Ultrafast spin-lasers, Nature (London) **568**, 212 (2019).

[14] J. F. G. Marin, D. Unuchek, Z. Sun, C. Y. Cheon, F. Tagarelli, K. Watanabe, T. Taniguchi, and A. Kis, Room-temperature electrical control of polarization and emission angle in a cavity-integrated 2D pulsed LED, Nat. Commun. **13**, 4884 (2022).

[15] K. Rong, X. Duan, B. Wang, D. Reichenberg, A. Cohen, C.-l. Liu, P. K. Mohapatra, A. Patsha, V. Gorovoy, S. Mukherjee, V. Kleiner, A. Ismach, E. Koren, and E. Hasman, Spin-valley Rashba monolayer laser, Nat. Mater. **22**, 1085 (2023).

[16] G. Y. Wu, N.-Y. Lue, and Y.-C. Chen, Quantum manipulation of valleys in bilayer graphene, Phys. Rev. B **88**, 125422 (2013).

[17] Z. Ye, D. Sun, and T. F. Heinz, Optical manipulation of valley pseudospin, Nat. Phys. **13**, 26 (2017).

[18] B. Huang, M. A. McGuire, A. F. May, D. Xiao, P. Jarillo-Herrero, and X. Xu, Emergent phenomena and proximity effects in two-dimensional magnets and heterostructures, Nat. Mater. **19**, 1276 (2020).

[19] D. Unuchek, A. Ciarrocchi, A. Avsar, K. Watanabe, T. Taniguchi, and A. Kis, Room-temperature electrical control of exciton flux in a van der Waals heterostructure, Nature (London) **560**, 340 (2018).

[20] I. Žutić, A. Matos-Abiague, B. Scharf, H. Dery, and K. Belashchenko, Proximitized materials, Mater. Today **22**, 85 (2019).

[21] I. Žutić, J. Fabian, and S. D. Sarma, Spintronics: Fundamantals and applications, Rev. Mod. Phys. **76**, 323 (2004).

[22] I. Vobornik, U. Manju, J. Fujii, F. Borgatti, P. Torelli, D. Krizmancic, Y. S. Hor, R. J. Cava, and G. Panaccione, Magnetic proximity effect as a pathway to spintronic applications of topological insulators, Nano Lett. **11**, 4079 (2011).

[23] A. I. Buzdin, Proximity effects in superconductor-ferromagnet heterostructures, Rev. Mod. Phys. **77**, 935 (2005).

[24] C. Zhao, T. Norden, P. Zhang, P. Zhao, Y. Cheng, F. Sun, J. P. Parry, P. Taheri, J. Wang, Y. Yang, T. Scrace, K. Kang, S. Yang, G.-X. Miao, R. Sabirianov, G. Kioseoglou, W. Huang, A. Petrou, and H. Zeng, Enhanced valley splitting in monolayer WSe_2 due to magnetic exchange field, Nat. Nanotechnol. **12**, 757 (2017).

[25] T. Hu, G. Zhao, H. Gao, Y. Wu, J. Hong, A. Stroppa, and W. Ren, Manipulation of valley pseudospin in WSe_2/CrI_3 heterostructures by the magnetic proximity effect, Phys. Rev. B **101**, 125401 (2020).

[26] T. Zhou, S. Cheng, M. Schleenvoigt, P. Schüffelgen, H. Jiang, Z. Yang, and I. Žutić, Quantum spin-valley Hall kink states: From concept to materials design, Phys. Rev. Lett. **127**, 116402 (2021).

[27] B. Scharf, G. Xu, A. Matos-Abiague, and I. Žutić, Magnetic proximity effects in transition-metal dichalcogenides: converting excitons, Phys. Rev. Lett. **119**, 127403 (2017).

[28] C. Gong and X. Zhang, Two-dimensional magnetic crystals and emergent heterostructure devices, Science **363**, eaav4450 (2019).

[29] D. Zhong, K. L. Seyler, X. Linpeng, N. P. Wilson, T. Taniguchi, K. Watanabe, M. A. McGuire, K.-M. C. Fu, D. Xiao, W. Yao, and X. Xu, Layer-resolved magnetic proximity effect in van der Waals heterostructures, Nat. Nanotechnol. **15**, 187 (2020).

[30] J. Choi, C. Lane, J.-X. Zhu, and S. A. Crooker, Asymmetric magnetic proximity interactions in $MoSe_2/CrBr_3$ van der Waals heterostructures, Nat. Mater. **22**, 305 (2023).

[31] T. Zhou and I. Žutić, Asymmetry in the magnetic neighbourhood, Nat. Mater. **22**, 284 (2023).

[32] C. Lee, F. Katmis, P. Jarillo-Herrero, J. S. Moodera, and N. Gedik, Direct measurement of proximity-induced magnetism at the interface between a topological insulator and a ferromagnet, Nat. Commun. **7**, 12014 (2016).

[33] G. Xu, T. Zhou, B. Scharf, and I. Žutić, Optically probing tunable band topology in atomic monolayers, Phys. Rev. Lett. **125**, 157402 (2020).

[34] F. Miao, S.-J. Liang, and B. Cheng, Straintronics with van der Waals materials, npj Quantum Mater. **6**, 59 (2021).

[35] R. Roldán, A. Castellanos-Gomez, E. Cappelluti, and F. Guinea, Strain engineering in semiconducting two-dimensional crystals, J. Phys.: Condens. Matter **27**, 313201 (2015).

[36] H. J. Conley, B. Wang, J. I. Ziegler, R. F. Haglund, Jr., S. T. Pantelides, and K. I. Bolotin, Bandgap engineering of strained monolayer and bilayer MoS_2, Nano Lett. **13**, 3626 (2013).

[37] K. He, C. Poole, K. F. Mak, and J. Shan, Experimental demonstration of continuous electronic structure tuning via strain in atomically thin MoS_2, Nano Lett. **13**, 2931 (2013).

[38] C. R. Zhu, G. Wang, B. L. Liu, X. Marie, X. F. Qiao, X. Zhang, X. X. Wu, H. Fan, P. H. Tan, T. Amand, and B. Urbaszek, Strain tuning of optical emission energy and polarization in monolayer and bilayer MoS_2, Phys. Rev. B **88**, 121301(R) (2013).

[39] Y. Wang, C. Cong, C. Qiu, and T. Yu, Raman spectroscopy study of lattice vibration and crystallographic orientation of monolayer MoS_2 under uniaxial strain, Small **9**, 2857 (2013).

[40] Z. Liu, M. Amani, S. Najmaei, Q. Xu, X. Zou, W. Zhou, T. Yu, C. Qiu, A. G. Birdwell, F. J. Crowne, R. Vajtai, B. I. Yakobson, Z. Xia, M. Dubey, P. M. Ajayan, and J. Lou, Strain and structure heterogeneity in MoS_2 atomic layers grown by chemical vapour deposition, Nat. Commun. **5**, 5246 (2014).

[41] Y. Wang, C. Cong, W. Yang, J. Shang, N. Peimyoo, Y. Chen, J. Kang, J. Wang, W. Huang, and T. Yu, Strain-induced direct-indirect bandgap transition and phonon modulation in monolayer WS_2, Nano Res. **8**, 2562 (2015).

[42] G. H. Ahn, M. Amani, H. Rasool, D.-H. Lien, J. P. Mastandrea, J. W. Ager, III, M. Dubey, D. C. Chrzan, A. M. Minor, and A. Javey, Strain-engineered growth of two-dimensional materials, Nat. Commun. **8**, 608 (2017).

[43] Y. Y. Hui, X. Liu, W. Jie, N. Y. Chan, J. Hao, Y.-T. Hsu, L.-J. Li, W. Guo, and S. P. Lau, Exceptional tunability of band energy in a compressively strained trilayer MoS_2 sheet, ACS Nano **7**, 7126 (2013).

[44] R. Frisenda, M. Drüppel, R. Schmidt, S. M. de Vasconcellos, D. P. de Lara, R. Bratschitsch, M. Rohlfing, and A. Castellanos-Gomez, Biaxial strain tuning of the optical properties of single-layer transition metal dichalcogenides, NPJ 2D Mater. Appl. **1**, 10 (2017).

[45] Z. Peng, X. Chen, Y. Fan, D. J. Srolovitz, and D. Lei, Strain engineering of 2D semiconductors and graphene: from strain fields to band-structure tuning and photonic applications, Light Sci. Appl. **9**, 190 (2020).

[46] Z. An, P. Soubelet, Y. Zhumagulov, M. Zopf, A. Delhomme, C. Qian, P. E. F. Junior, J. Fabian, X. Cao, J. Yang, A. V. Stier, F. Ding, and J. J. Finley, Strain control of exciton and trion spin-valley dynamics in monolayer transition metal dichalcogenides, Phys. Rev. B **108**, L041404 (2023).

[47] J. Zhang, S. Jia, I. Kholmanov, L. Dong, D. Er, W. Chen, H. Guo, Z. Jin, V. B. Shenoy, L. Shi, and J. Lou, Janus monolayer transition-metal dichalcogenides, ACS Nano **11**, 8192 (2017).

[48] A.-Y. Lu, H. Zhu, J. Xiao, C.-P. Chuu, Y. Han, M.-H. Chiu, C.-C. Cheng, C.-W. Yang, K.-H. Wei, Y. Yang, Y. Wang, D. Sokaras, D. Nordlund, P. Yang, D. A. Muller, M.-Y. Chou, X. Zhang, and L.-J. Li, Janus monolayers of transition metal dichalcogenides, Nat. Nanotechnol. **12**, 744 (2017).

[49] T. Hu, F. Jia, G. Zhao, J. Wu, A. Stroppa, and W. Ren, Intrinsic and anisotropic Rashba spin splitting in Janus transition-metal dichalcogenide monolayers, Phys. Rev. B **97**, 235404 (2018).

[50] D. Xiao, G.-B. Liu, W. Feng, X. Xu, and W. Yao, Coupled spin and valley physics in monolayers of MoS_2 and other group-VI dichalcogenides, Phys. Rev. Lett. **108**, 196802 (2012).

[51] J. Qi, X. Li, Q. Niu, and J. Feng, Giant and tunable valley degeneracy splitting in $MoTe_2$, Phys. Rev. B **92**, 121403(R) (2015).

[52] H. Rostami, R. Roldán, E. Cappelluti, R. Asgari, and F. Guineam, Theory of strain in single-layer transition metal dichalcogenides, Phys. Rev. B **92**, 195402 (2015).

[53] A. J. Pearce, E. Mariani, and G. Burkard, Tight-binding approach to strain and curvature in monolayer transition-metal dichalcogenides, Phys. Rev. B **94**, 155416 (2016).

[54] S. Fang, S. Carr, M. A. Cazalilla, and E. Kaxiras, Electronic structure theory of strained two-dimensional materials with hexagonal symmetry, Phys. Rev. B **98**, 075106 (2018).

[55] Y. A. Korkmaz, C. Bulutay, and C. Sevik, k · p parametrization and linear and circular dichroism in strained monolayer (Janus) transition metal dichalcogenides from first-principles, J. Phys. Chem. C **125**, 7439 (2021).

[56] J. D. Cao, G. Xu, B. Scharf, K. Denisov, and I. Žutić, Emergent bright excitons with Rashba spin-orbit coupling in atomic monolayers, Phys. Rev. B **109**, 085407 (2024).

[57] M. Rohlfing and S. G. Louie, Electron-hole excitations and optical spectra from first principles, Phys. Rev. B **62**, 4927 (2000).

[58] B. Scharf, T. Frank, M. Gmitra, J. Fabian, I. Žutić, and V. Perebeinos, Excitonic Stark effect in MoS_2 monolayers, Phys. Rev. B **94**, 245434 (2016).

[59] C. Zhang, H. Wang, W. Chan, C. Manolatou, and F. Rana, Absorption of light by excitons and trions in monolayers of metal dichalcogenide MoS_2: Experiments and Theory, Phys. Rev. B **89**, 205436 (2014).

[60] D. V. Tuan, B. Scharf, Z. Wang, J. Shan, K. F. Mak, I. Žutić, and H. Dery, Probing many-body interactions in monolayer transition-metal dichalcogenides, Phys. Rev. B **99**, 085301 (2019).

[61] Y.-H. Chu, L. W. Martin, M. B. Holcomb, M. Gajek, S.-J. Han, Q. He, N. Balke, C.-H. Yang, D. Lee, W. Hu, Q. Zhan, P.-L. Yang, A. Fraile-Rodríguez, A. Scholl, S. X. Wang, and R. Ramesh, Electric-field control of local ferromagnetism using a magnetoelectric multiferroic, Nat. Mater. **7**, 478 (2008).

[62] D. A. Bussian, S. A. Crooker, M. Yin, M. Brynda, A. L. Efros, and V. I. Klimov, Tunable magnetic exchange interactions in manganese-doped inverted core-shell ZnSe-CdSe nanocrystals, Nat. Mater. **8**, 35 (2009).